

Orbital-selective spin excitation of a magnetic porphyrin

C. Rubio-Verdú,¹ A. Sarasola,^{2,3} D. -J. Choi,¹ Z. Majzik,¹ R. Ebeling,¹ M. R. Calvo,^{1,4} M. M. Ugeda,^{1,4} A. García-Lekue,^{2,4} D. Sánchez-Portal,^{2,5} and J. I. Pascual^{1,4}

¹*CIC nanoGUNE, 20018 Donostia-San Sebastián, Spain*

²*Donostia International Physics Center (DIPC), 20018 Donostia-San Sebastián, Spain*

³*Faculty of Engineering, Gipuzkoa, 20018 Donostia-San Sebastián, Spain*

⁴*Ikerbasque, Basque Foundation for Science, Bilbao, Spain*

⁵*Centro de Física de Materiales (CFM), 20018 Donostia-San Sebastián, Spain*

(Dated: July 21, 2022)

We study the intramolecular dependence of spin excitations in Fe porphyrin molecules on a Au(111) surface using spatially-resolved Scanning Tunneling Spectroscopy. Our results reveal a spin transition that spreads along one molecular axis with distinct lineshapes at on- and off-center locations. Simulations of the spectral fingerprints with a phenomenological scattering model point to significant spatial variations of the spin-electron scatterings mechanisms. We deduce that, at each location, the spin excitation is predominantly driven by each of the two competing tunnel-assisted channels, associated to two different frontier electronic states. With the support of Density Functional Theory simulations, we identify these as molecular resonances with high spectral weight of Fe spin-polarized orbitals and of metal-pyrrole hybrid states, respectively. We thus show that the electron scattering pathways mediating spin excitation can be tuned by selecting the site of electron injection within the molecule.

PACS numbers: 68.37.Ef, 75.30.Gw, 75.50.Xx, 71.15.Mb, 72.15.Qm

The survival of a net spin in magnetically doped metal-organic molecules is the fundamental requirement for their application in molecular spintronics [1–3]. Spin currents [4], tunable magneto-transport, or organic spin valves [5] have been realized in magnetic-organic materials. In most of the cases, the functionality of the device relies on fundamental aspects about the interaction of electron currents with spins. However, the mechanisms behind spin-electron coupling depend on multiple parameters such as the overlap of metal and ligand states, the symmetry of the ligand environment and the level of occupation [6]. Thus a molecular scale picture connecting conformational, electronic and spin states of a molecule, as well as describing interactions with the environment, is generally required [6–8].

In this context, Scanning Tunneling Microscopy (STM) combined with Density Functional Theory (DFT) succeeded in unveiling spin properties of materials with high spatial and energy precision. In particular, studies of prototypical systems such as transition-metal (TM) porphyrins and phtalocyanines, found that the spin of the TM atom is modified by the organic ligands and becomes partially extended into delocalized molecular states [9]. Furthermore, the organic ligands favor a net spin orientation by inducing an intrinsic magnetic anisotropy [10]. Identification of these mechanisms is, however, generally distracted by spurious spin-modification effects induced by strong interactions with supporting electrodes [6, 11–18]. Such interactions induce scattering, screen molecular spins via the Kondo effect [11], introduce charge transfer [19], lead to orbital-specific hybridization [20] and induce conformational changes of the molecular structure [8].

Here, we investigate Fe-tetraphenyl porphyrin

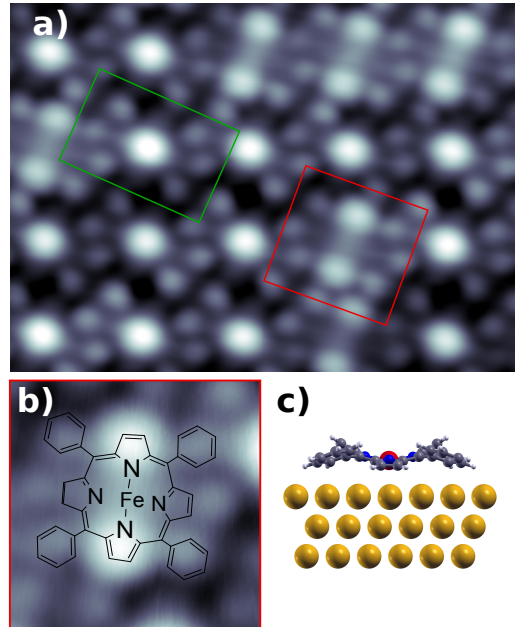


FIG. 1: (a) Topographic STM image ($7 \times 5 \text{ nm}^2$) of a close-packed island of FeTPP (red box) and FeTPP-Cl (green box) molecules on Au(111). Imaging conditions: $V = 0.25 \text{ V}$, $I = 10 \text{ pA}$. (b) Zoom of a single FeTPP molecule and molecular structure superimposed. (c) Cross section of the DFT relaxed structure of the FeTPP on the Au(111) surface (3 gold layers) showing the saddle conformation acquired upon adsorption.

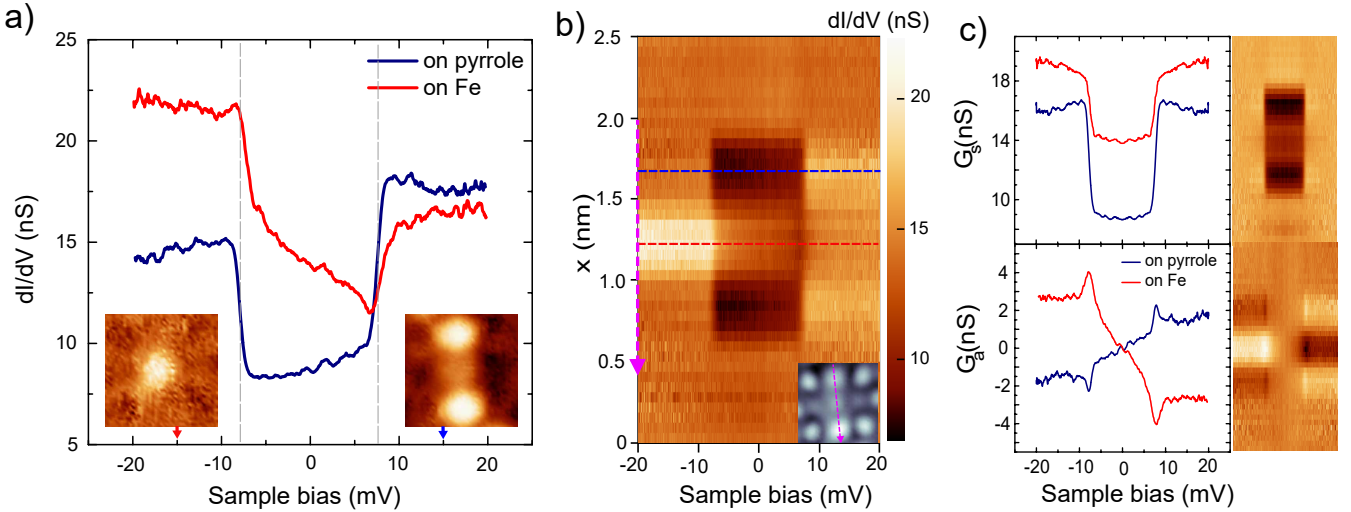


FIG. 2: (a) dI/dV spectra of FeTPP measured over the pyrrole groups (blue) and over the central Fe ion (red) (setpoint: $V = 20$ mV, $I = 300$ pA. Lock-in frequency 938 Hz, modulation 50 μ V rms). The insets are 1.7×1.7 nm 2 constant current dI/dV maps at $V = -15$ mV and $V = +15$ mV of the topography image shown as inset in (b). (b) Stacking plot of point dI/dV spectra (40 curves, 2.5 nm) along the axis of a FeTPP molecule (as shown in the inset). (c) Symmetric ($G_s = \frac{1}{2}(G_{V>0} + G_{V<0})$) and antisymmetric ($G_a = \frac{1}{2}(G_{V>0} - G_{V<0})$) components of the dI/dV spectra of (a) and their flatten spatial distribution along the axis of the FeTPP molecule, as in (b).

(FeTPP) molecules adsorbed on a Au(111) surface by Scanning Tunneling Spectroscopy (STS). We find that the intrinsic magnetic moment $S = 1$ of FeTPP remains unquenched on the surface and detectable through its low-energy spin excitations. By spatially mapping the excitations, we find them spread over the Fe ion and two of the four molecular pyrrole groups. We show that the molecular spin can be inelastically excited by electrons tunneling through two different molecular orbitals. The inelastic scattering mechanism differs for each channel and is manifested as different STS lineshapes. DFT simulations describe the two channels as two distinct spin-polarized molecular states with strong Fe character and different distribution within the molecule. Our results highlight the possibility of interpreting magnetic fingerprints in terms of the alignment and hybridization of the molecular states hosting the molecular spin.

Our experiments were performed in a SPECS JT-STM with a base temperature of 1.1 K under UHV conditions. We thermally sublimated 5,10,15,20-tetraphenylporphine iron(III) chloride (FeTPP-Cl) molecules on the clean Au(111) substrate at room temperature. Differential conductance (dI/dV) measurements were acquired using lock-in amplifier technique.

STM images show that the porphyrin molecules arrange in close-packed islands on the Au(111) surface (Fig. 1(a)) and appear with a protrusion at the center (green box in Fig. 1(a)) that is attributed to the Cl ligand of the intact FeTPP-Cl molecule. A fraction of the molecules exhibits instead two lobes that we identify as the dechlorinated species FeTPP (Fig. 1(b)). They can also be

obtained by removing the Cl ligand from the FeTPP-Cl molecules using tunneling electrons or by annealing the substrate [6]. The dechlorination process changes the Fe oxidation state from Fe⁺³ to Fe⁺² and decreases the total spin from $S = 3/2$ to $S = 1$ [6, 7, 21].

In the following we focus on the dechlorinated FeTPP species. STS measurements over the molecules reveal steps in conductance at symmetric bias values (Fig. 2(a)), a fingerprint of spin excitations induced by tunneling electrons [7, 22–25]. We find a striking spatial distribution of the spectroscopic features (see Fig. 2(a)). While the energy position of the inelastic conductance steps remains the same ($V_s = \pm 7.4 \pm 0.5$ mV) all over the molecule, their symmetry varies as we move off-center towards the brighter pyrroles. A stacking plot of point dI/dV spectra across the FeTPP molecule (Fig. 2(b)) shows inelastic steps with a rather symmetric lineshape over the pyrroles and with strong antisymmetric character over the Fe site. It is remarkable that the energy positions of the conductance steps remain nevertheless constant, indicating that the same excitation is the origin for the inelastic features across the molecule. The spin excitation is only observed along the axis formed by the brighter pyrroles (marked in inset in Fig. 2(b)), and is absent over the two other pyrroles (see Figure S3 in Supplemental Material (SM) [26]).

In a first approximation, the spin-flip excitation energy is just determined by the magnetic anisotropy of the molecule on the surface, which can be modeled with a phenomenological spin Hamiltonian [27] $\hat{H}_s = D\hat{S}_z^2 + E(\hat{S}_x^2 - \hat{S}_y^2)$, where $\hat{S}_x, \hat{S}_y, \hat{S}_z$ are the three components

of the spin operator, and D and E the axial and transverse anisotropy parameters, respectively. We associate the excitation at $V_s = \pm 7.4$ mV with a transition from the $|m_S = 0\rangle$ ground state to the $|m_S = \pm 1\rangle$ multiplet. A single step is an indication of $E = 0$ and the excitation energy is then a direct measure of the axial anisotropy constant, $D = 7.4$ meV. This value is close to that reported for FeTPP crystals [28], and smaller than that found for octaethyl-Fe-porphine on Au(111) [6]. About 15% of the molecules exhibit the inelastic step split in two smaller steps, at $V_s = \pm 8.7$ and ± 6.5 mV (see Figure S4 in SM [26]). This is in agreement with an integer spin configuration under finite transverse anisotropy constant E , probably due to small distortions of the molecular structure on the surface site [7].

While the above spin-model successfully predicts excitation energies and transition rates [27], spin-electron interactions must be taken into account to fully describe inelastic tunneling through these systems. Electron scattering mechanisms contributing to the inelastic signal can be described by Hamiltonian terms of the form $H_{int} \simeq \mathcal{U} + \mathbf{J} \cdot \mathbf{s} \cdot \mathbf{S}$. The exchange term J describes the transfer of energy and angular momentum by electrons (with spin \mathbf{s}), and accounts for excitations of the molecular spin \mathbf{S} . The potential term \mathcal{U} reflects charge scattering processes by partially occupied localized states [29, 30], and its role has typically been disregarded in magnetic systems.

Most of the scattering processes contribute to the tunneling conductance with bias-symmetric components. However, it has been recently shown [30] that high-order processes associated to a finite potential scattering term introduce an antisymmetric behavior in the spectra. Following this interpretation, we separate the symmetric G_s and antisymmetric G_a parts of the spectra in Fig. 2(a) as indicated in the caption. The resulting plots (Fig. 2(c)) reveal that the inelastic fraction in the symmetric component is larger over the pyrrole groups by a factor of 3 (inelastic fraction $\frac{\Delta G_a}{G_s}$ amounts to 0.9 and 0.3 over pyrroles and Fe, respectively), while the antisymmetric component G_a has opposite sign on each site, and is 2 times larger over the Fe ion. Furthermore, the G_a component shows characteristic dips and peaks at the onset of excitation, which closely resemble the shape of higher order terms associated to a non-zero potential scattering amplitude in inelastic co-tunneling calculations [30]. We thus fitted the dI/dV spectra of Fig. 2(a) using a (second-order scattering) phenomenological model developed by Ternes [30] (for fit results see Figure S1 in SM [26]). The stronger antisymmetric component of the curve taken over the Fe ion is reproduced using a large and positive ratio between potential and exchange scattering amplitudes, i.e. $U = \mathcal{U}/J = 0.8$, whereas the opposite and weaker antisymmetric component of the curve taken on the pyrroles is due to a smaller and negative ratio, $U = -0.4$.

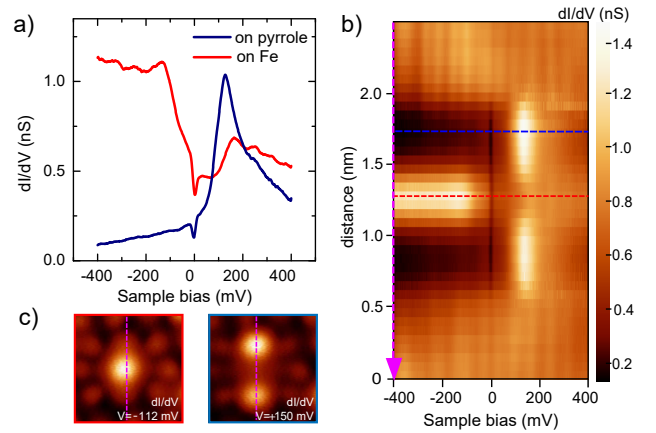


FIG. 3: (a) dI/dV spectra of FeTPP measured on the two bright pyrrole groups (blue) and on the central Fe atom (red) (setpoint: $V = 0.4$ V, $I = 300$ pA. Lock-in frequency 938 Hz, modulation 2 mV rms). The spectra is measured in a wider range as in Fig. 2(a) to capture the shape and position of frontier orbitals. (b) Stacking plot of point dI/dV spectra (40 curves, 2.5 nm) along the FeTPP molecule showing the spatial localization of dI/dV signal along the axis determined by the two bright pyrroles. (c) Constant height conductance maps at the energy of the resonances observed in (a).

The microscopic Anderson model [29–31] provides a physical interpretation for the phenomenological parameter U obtained from the fit to the experimental spectra. As described by the Schrieffer-Wolff transformation [29], U depends linearly on the ratio between energy position of the singly occupied spin state and the on-site Coulomb energy ϵ_d/U_d . For the more symmetric STS lineshape taken on the pyrroles we obtain $\epsilon_d = -0.7U_d$, which can be interpreted as a spin state close to the electron-hole symmetry point ($\epsilon_d = -0.5U_d$), where potential scattering would be absent ($U = 0$). In contrast, from spectra on the Fe site we obtain $\epsilon_d = -0.1U_d$ a situation where the spin is close to the mixed-valence regime and the potential scattering is significant.

Although both scenarios deviate from the electron-hole symmetry point, on the central Fe ion the situation is extreme and, therefore, the spectra shows a larger antisymmetric component. Even if the Anderson model does not capture the complexity of the spin density distribution of a metal-organic system, it still provides a suitable interpretation for our data. While the spin density must be mostly located on the Fe atom, the excitation can be driven by tunneling into two non-degenerated orbitals with different spatial distribution.

The energy alignment of the FeTPP frontier orbitals can be explored in spectra measured in a wider bias range. In consistency with the above-described picture, we find two electronic resonances around the Fermi level, each showing a different linewidth and spatial dependence (Fig. 3(a)). While a sharp resonance appears at

$V_S = +150$ mV on the pyrroles, a broad state is found at negative bias over the Fe site. The dI/dV stacking plot along the molecular axis (Fig. 3(b)) captures these differences, and reveals an orbital pattern similar to that of the spin excitations (Fig. 2(b)). The dI/dV maps in Fig. 3(c) further localize the positive and negative frontier orbitals along two of the four pyrroles and over the Fe center, respectively. This agrees with a molecular symmetry breaking, also observed in the spin excitation maps (Fig. 2(a)). We note that the broad negative-bias resonance on the Fe ion crosses through zero bias, revealing a situation close to the mixed-valence regime, in agreement with the outcome of the Anderson model from above.

In order to identify the orbital character of the frontier spectral features of FeTPP on Au(111) we analyzed its electronic configuration and spin state by means of DFT simulations based on the SIESTA code [32]. We find that adding a Hubbard-like term with $U_d = 2$ eV to describe the Coulomb interactions between electrons in the Fe $3d$ shell is crucial to reproduce the orbital alignment around E_F observed in the experiment [33]. For the free-standing molecule, our results confirm the well-known multi-configurational character of the ground state of FeTPP [34, 35]. Correspondingly, we found almost degenerate solutions with quite different fillings of the levels associated with the metallic center and the same total spin. On the Au(111) surface the molecule adopts a distorted saddle configuration, as previously reported for porphyrins on surfaces [8]. Figure 4(a) shows the density of states of FeTPP/Au(111) projected on Fe d orbitals (PDOS). The FeTPP on Au(111) has a total spin $S = 1$ shared between frontier states, which have strong character on d_{z^2} and d_{π} orbitals of the Fe ion (see the sketch in Figure 4(b)). The d_{xy} and $d_{x^2-y^2}$ -derived states are fully occupied and empty, respectively, and largely localized due to their weak interaction with the metal substrate. The d_{z^2} -derived state has a net spin polarization of $0.75 \mu_B$ and is quite broad as a consequence of its large hybridization with the substrate. The d_{π} -derived states appear with a broken degeneracy caused by the saddle-like distortion of the molecular backbone on the substrate. The lowest energy configuration finds d_{yz} orbital with larger spin density, while the d_{xz} is almost completely occupied and, thus, exhibits a substantially smaller spin polarization. Namely, the spin polarization coming from the d_{π} orbitals is dominated by the contribution from d_{yz} . The computed PDOS thus pictures the multi-orbital character of the spin polarization of this system.

The spatial spin excitation pattern observed in the experiment is a consequence of different molecular states involved in the tunneling through the molecule. In Fig. 4(c) we compare PDOS on the orbitals of Fe and those of the atoms in the upper-pyrrole groups. The former resemble the dI/dV spectrum at the center of the molecule

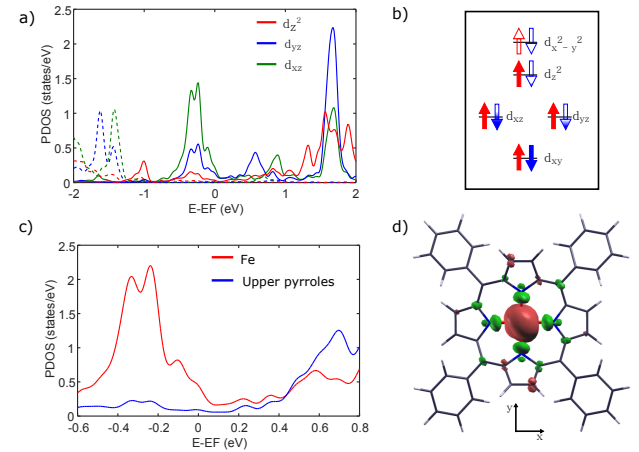


FIG. 4: (a) Spin-polarized DOS of the FeTPP/Au(111) system projected on Fe d_{xz} , d_{yz} and d_{z^2} orbitals (dashed/solid lines represent majority/minority spin states). (b) Simplified scheme describing the occupation of Fe 3d levels for the adsorbed FeTPP (red/blue arrows indicate majority/minority spin states). The different occupation of each state is indicated by the color filling of the corresponding arrows. (c) Total DOS of the FeTPP/Au(111) system projected on Fe states and on C and N states of the upper pyrrole moieties. (d) Spin polarization isosurface obtained for the FeTPP/Au(111) system by subtracting occupied states with spin up and down (red/green surfaces describe majority/minority spin states; upper pyrroles are at the top & bottom of the structure; the Au(111) surface has been omitted from the plot for clarity).

in Fig. 3(a), with larger DOS at the negative part of the energy spectrum plus some weight above E_F . Thus, the tunneling transmission on the Fe ion is governed by Fe states, probably via the broad d_{z^2} components, which extend further into the vacuum. The overlap of these states at E_F also agrees with a configuration closer to a mixed-valence regime, as concluded from the phenomenological interpretation of the antisymmetric excitation lineshape at the Fe site. In contrast, the PDOS on the upper-pyrrole states exhibit only a resonance at positive energy, which correlates with the dI/dV spectra measured over the protruding pyrrole groups (Fig. 3(a)). The saddle distortion of the molecule reduces the direct interaction of the upper pyrroles with the surface. However, the ligand state overlaps with the empty d_{yz} component of the Fe ion, acquiring a hybrid Fe-ligand character and, as a consequence, becoming weakly spin-polarized (Fig. 4(d)). Therefore, tunneling through pyrrole-Fe hybrid states can effectively excite the spin of the Fe ion, whereas the smaller overlap of this resonance with E_F agrees with the more symmetric excitation lineshape observed in the experiment.

In summary, we reported the spatial dependence of inelastic spin excitations of a FeTPP molecule on a Au(111) surface. We found that the associated spectral lineshape appears with antisymmetric components, reflecting the

strength of higher order scattering components of the inelastic tunneling process. Interpreting our STS results with the support of phenomenological scattering models and with first principle simulations, we unravel the existence of two distinct tunneling channels mediating the inelastic spin excitation. At the center of the molecule, a large potential scattering featured by occupied Fe d states close to E_F leads to highly antisymmetric components. On the off-center pyrrole groups, a spin-polarized molecular state mixed with Fe d_{yz} character shows a weaker interaction with the metal and, therefore, larger symmetric components. Our results demonstrate that the same spin transition can be selectively excited through two different tunneling channels due to their distinct energy and spatial distribution.

We thank Nicolás Lorente and Thomas Frederiksen for stimulating discussions. This work has been funded by the COST 15128 Molecular Spintronics project, by Marie Curie IF ARTE, by the Spanish Ministerio de Economía y Competitividad (MINECO) through the cooperative grant No. MAT2016-78293 and grant No. FIS2016-75862-P, and by the Basque Government (Dep. Industry, Grant PI-2015-1-42, Dep. Education, Grant PI-2016-1-27 and Grant IT-756-13), the EU project PAMS (610446), and the European Regional Development Fund (ERDF).

[1] C. Joachim, J. K. Gimzewski, and A. Aviram, *Nature* **408**, 541 (2000).
[2] S. A. Wolf, *Science* **294**, 1488 (2001).
[3] L. Bogani and W. Wernsdorfer, *Nat. Mater.* **7**, 179 (2008).
[4] V. A. Dedić, L. E. Hueso, I. Bergenti, and C. Taliani, *Nat. Mater.* **8**, 707 (2009).
[5] S. Schmaus, A. Bagrets, Y. Nahas, T. K. Yamada, A. Bork, M. Bowen, E. Beaurepaire, F. Evers, and W. Wulfhekel, *Nat. Nanotech.* **6**, 185 (2011).
[6] B. W. Heinrich, G. Ahmadi, V. L. Müller, L. Braun, J. I. Pascual, and K. J. Franke, *Nano Lett.* **13**, 4840 (2013).
[7] B. W. Heinrich, L. Braun, J. I. Pascual, and K. J. Franke, *Nano Lett.* **15**, 4024 (2015).
[8] W. Auwärter, D. Écija, F. Klappenberger, and J. V. Barth, *Nat. Chem.* **7**, 105 (2015).
[9] A. Strózecka, A. Eiguren, and J. I. Pascual, *Phys. Rev. Lett.* **107** (2011).
[10] D.-S. Wang, R. Wu, and A. J. Freeman, *Physical Review B* **47**, 14932 (1993).
[11] A. Zhao, Q. Li, L. Chen, H. Xiang, W. Wang, S. Pan, B. Wang, X. Xiao, J. Yang, J. G. Hou, and Q. Zhu, *Science* **309**, 1542 (2005).

[12] U. G. E. Perera, H. J. Kulik, V. Iancu, L. G. G. V. Dias da Silva, S. E. Ulloa, N. Marzari, and S.-W. Hla, *Phys. Rev. Lett.* **105** (2010).
[13] L. Gao, W. Ji, Y. B. Hu, Z. H. Cheng, Z. T. Deng, Q. Liu, N. Jiang, X. Lin, W. Guo, S. X. Du, W. A. Hofer, X. C. Xie, and H.-J. Gao, *Phys. Rev. Lett.* **99** (2007).
[14] A. Zhao, Z. Hu, B. Wang, X. Xiao, J. Yang, and J. G. Hou, *J. Chem. Phys.* **128**, 234705 (2008).
[15] W. Wang, R. Pang, G. Kuang, X. Shi, X. Shang, P. N. Liu, and N. Lin, *Phys. Rev. B* **91** (2015).
[16] J. J. Parks, A. R. Champagne, T. A. Costi, W. W. Shum, A. N. Pasupathy, E. Neuscamman, S. Flores-Torres, P. S. Cornaglia, A. A. Aligia, C. A. Balseiro, G. K.-L. Chan, H. D. Abruna, and D. C. Ralph, *Science* **328**, 1370 (2010).
[17] V. Iancu, A. Deshpande, and S.-W. Hla, *Nano Lett.* **6**, 820 (2006).
[18] V. Iancu, A. Deshpande, and S.-W. Hla, *Phys. Rev. Lett.* **97**, 266603 (2006).
[19] A. Mugarza, R. Robles, C. Krull, R. Korytár, N. Lorente, and P. Gambardella, *Phys. Rev. B* **85** (2012).
[20] P. Gargiani, G. Rossi, R. Biagi, V. Corradini, M. Pedio, S. Fortuna, A. Calzolari, S. Fabris, J. C. Cezar, N. B. Brookes, and M. G. Betti, *Phys. Rev. B* **87** (2013).
[21] T. G. Gopakumar, H. Tang, J. Morillo, and R. Berndt, *J. Am. Chem. Soc.* **134**, 11844 (2012).
[22] B. C. Stipe, M. A. Rezaei, and W. Ho, *Science* **280**, 1732 (1998).
[23] A. J. Heinrich, J. A. Gupta, C. P. Lutz, and D. M. Eigler, *Science* **306**, 466 (2004).
[24] B. W. Heinrich, G. Ahmadi, V. L. Müller, L. Braun, J. I. Pascual, and K. J. Franke, *Nano Lett.* **13**, 4840 (2013).
[25] B. W. Heinrich, L. Braun, J. I. Pascual, and K. J. Franke, *Nat. Phys.* **9**, 765 (2013).
[26] See Supplemental Material at [URL will be inserted by publisher].
[27] D. Gatteschi, R. Sessoli, and J. Villain, *Molecular nanomagnets*, 5 (Oxford University Press, 2006).
[28] P. D. Boyd, D. A. Buckingham, R. F. McMeeking, and S. Mitra, *Inor. Chem.* **18**, 3585 (1979).
[29] J. R. Schrieffer and P. A. Wolff, *Phys. Rev.* **149**, 491 (1966).
[30] M. Ternes, *New J. Phys.* **17**, 063016 (2015).
[31] P. W. Anderson, *Phys. Rev.* **124**, 41 (1961).
[32] J. M. Soler, E. Artacho, J. D. Gale, A. García, J. Junquera, P. Ordejón, and D. Sánchez-Portal, *J. Phys. Condens. Matter* **14**, 2745 (2002).
[33] I. E. Brumboiu, S. Haldar, J. Lüder, O. Eriksson, H. C. Herper, B. Brena, and B. Sanyal, *J. Chem. Theory Comput.* **12**, 1772 (2016).
[34] S. Vancoillie, H. Zhao, V. T. Tran, M. F. A. Hendrickx, and K. Pierloot, *J. Chem. Theory Comput.* **7**, 3961 (2011).
[35] M.-S. Liao, J. D. Watts, and M.-J. Huang, *J. of Phys. Chem. A* **111**, 5927 (2007).

Supplemental Material

Orbital-selective spin excitation of a magnetic porphyrin

C. Rubio-Verdú,¹ A. Sarasola,^{2,3} D. -J. Choi,¹ Z. Majzik,¹ R. Ebeling,¹ M. R. Calvo,^{1,4} M. M. Ugeda,^{1,4} A. García-Lekue,^{2,4} D. Sánchez-Portal,^{2,5} and J.I. Pascual^{1,4}

¹*CIC nanoGUNE, 20018 Donostia-San Sebastián, Spain*

²*Donostia International Physics Center (DIPC), 20018 Donostia-San Sebastián, Spain*

³*Faculty of Engineering, Gipuzkoa, 20018 Donostia-San Sebastián, Spain*

⁴*Ikerbasque, Basque Foundation for Science, Bilbao, Spain*

⁵*Centro de Física de Materiales (CFM), 20018 Donostia-San Sebastián, Spain*

PACS numbers: 68.37.Ef, 75.30.Gw, 75.50.Xx, 71.15.Mb, 72.15.Qm

HIGH-ORDER SCATTERING MODEL FOR SPIN EXCITATIONS

The energy spectrum of an atomic spin on a surface can be described by a Hamiltonian which includes single-spin H_s [S1] and spin-surface interaction H_{int} terms [S2, S3] as showed in the main text (we will follow the notation in Ref. [S4]). We fitted our experimental STS curves to a higher-order scattering model using the software provided by Ternes [S4] (Figure S1).

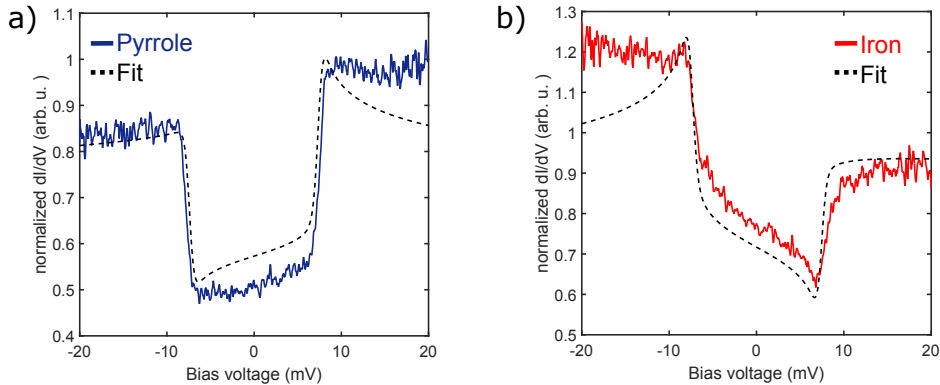


FIG. S1: (a) dI/dV spectra of FeTPP measured on the pyrrole (solid line) and the fitting results (dashed line) (b) dI/dV spectra of FeTPP measured on the Fe (solid line) and the fitting results (dashed line).

The Schrieffer-Wolff transformation [S3], provides a microscopic description of our system in terms of the single-impurity Anderson model. The energy position of the singly occupied spin state ϵ_d and the on-site Coulomb energy U_d are given by the expressions:

$$J = \frac{2}{\pi} \Delta^2 \left(\frac{1}{\epsilon_d} - \frac{1}{\epsilon_d + U_d} \right) \quad (S1)$$

$$\mathcal{U} = \frac{2}{\pi} \Delta^2 \left(\frac{1}{\epsilon_d} + \frac{1}{\epsilon_d + U_d} \right) \quad (S2)$$

where Δ is the broadening of the occupied state due to hybridization with the substrate, J the Kondo spin-spin exchange scattering and \mathcal{U} the potential scattering amplitude. While J is always negative, \mathcal{U} can take either sign.

The fits yield the ratio between potential and exchange scattering, represented by the adimensional parameter $U = \mathcal{U}/J$ [S4]. From this parameter and using the Schrieffer-Wolff transformation, we can extract the ratio $-\epsilon_d/U_d$ for the pyrrole and iron site:

$$U = \frac{\mathcal{U}}{J} = \frac{\frac{1}{\epsilon_d} + \frac{1}{\epsilon_d + U_d}}{\frac{1}{\epsilon_d} - \frac{1}{\epsilon_d + U_d}} = \frac{U_d + 2\epsilon_d}{U_d} = 1 + 2\frac{\epsilon_d}{U_d} \quad (S3)$$

The corresponding parameters for both pyrrole and iron sites are summarized in Table I (with fixed $T_0^2 = 0.15$, the background conductance $\sigma_0 = 3.5$ and the effective temperature $T_{eff} = 2.2$ K equal for both sites).

position	D (meV)	U	$\rho_s J$	$-\epsilon_d/U_d$
pyrrole	7.4	-0.4	-0.2	0.7
iron	7.4	0.8	-0.2	0.1

TABLE I: Fitting parameters for the experimental results shown in Figure S1

The relation $\epsilon_d = -xU_d$ conveys information about the relative alignment of the spin energy levels with respect to the Fermi energy of the surface. The situation $x=0.5$ represents the electron-hole symmetry in the Anderson model, while $x=0$ and $x=1$ represent the spin level and the excited states aligned at the Fermi energy respectively. In Figure S2 we show a sketch of the values extracted from the fit.

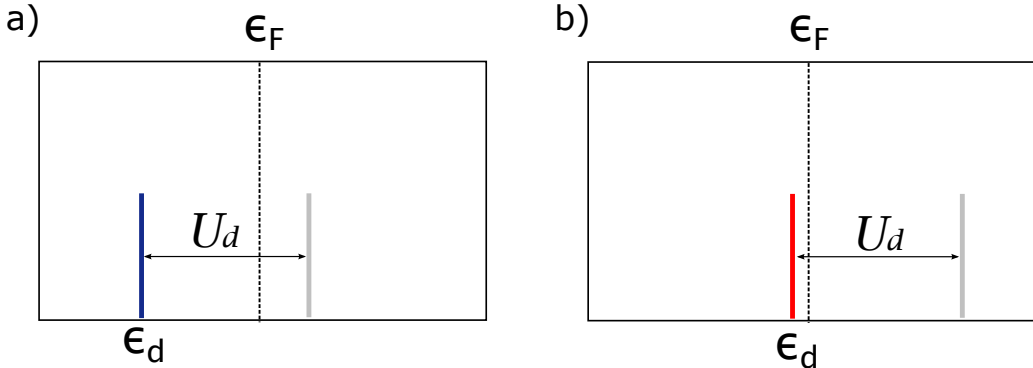


FIG. S2: Representation of the single-impurity Anderson model parameters for the values obtained from the fits to the experimental spectra for (a) pyrroles $\epsilon_d/U_d = -0.7$ and (b) iron site $\epsilon_d/U_d = -0.1$

SPIN EXCITATION LOCALIZED ALONG ONE AXIS OF THE FeTPP

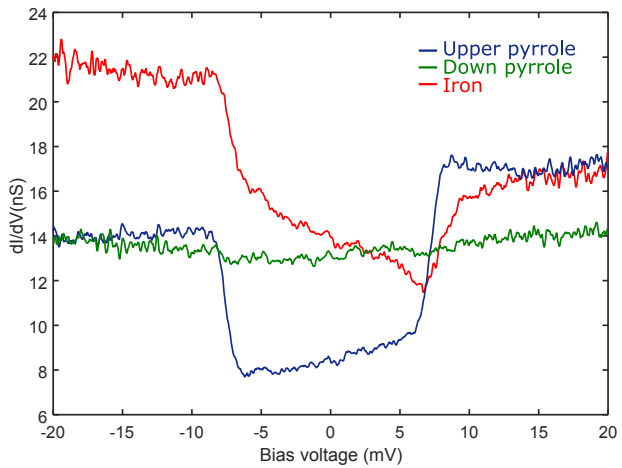


FIG. S3: dI/dV spectra over the two types of pyrroles and on the Fe position in the FeTPP molecule.

Figure S3 shows that the behavior is very different over the upper and lower pyrrole groups. As discussed in the main text, the spin can be excited along one molecular axis. As a consequence, spectra over the upper pyrroles show the spin excitation at $V_{bias} = \pm 7.4 \pm 0.5$ mV while the other pyrroles show no features around Fermi energy.

FeTPP IN THE PRESENCE OF TRANSVERSE ANISOTROPY

We found that $\sim 15\%$ of the FeTPP molecules showed the spin excitation step split into two smaller steps separated by $\Delta V_S \leq 2$ mV (Figure S4). This split signals the existence of a finite transverse anisotropy E for these molecules, probably caused by small conformational distortions. In Figure S4 we also show the fit [S5] of the experimental dI/dV curves but now including a transverse anisotropy parameter $E = 1$ meV.

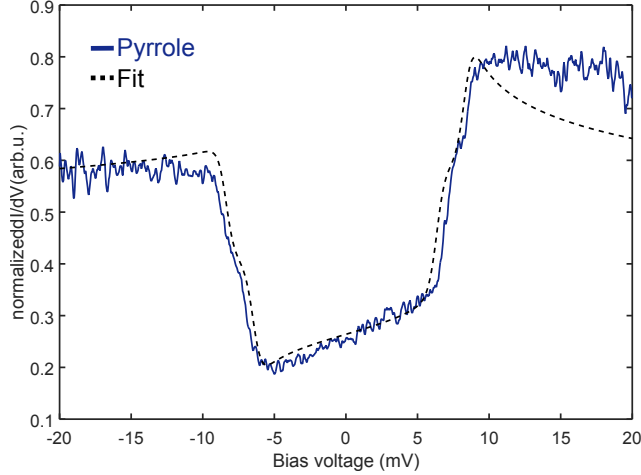


FIG. S4: dI/dV spectrum showing the zero-field split spin excitation due to the presence of transverse magnetic anisotropy E .

ORBITAL DISTRIBUTION OF THE FeTPP

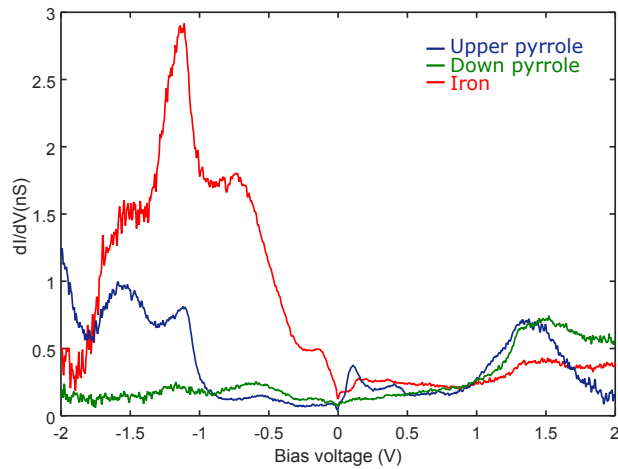


FIG. S5: Wider range dI/dV spectra on the two types of pyrroles and on the Fe position in the FeTPP molecule.

Figure S5 shows the wider bias range dI/dV spectra over the upper pyrrole, the down pyrrole and the Fe atom of the FeTPP molecule.

DETAILS ON THEORETICAL CALCULATIONS

Ab initio Density Functional Theory calculations were carried out using the generalized gradient approximation (GGA) with the Hubbard-like U_d correction as proposed by Dudarev [S6] and as implemented in the 4.1 version of SIESTA code [S7]. The optB88-vdW [S8] version of the non-local van der Waals potential is included to describe the exchange-correlation. For the description of the molecules on the substrate we considered a supercell made up of a 3 layer Au(111) slab, with a FeTPP molecule placed at its most stable adsorption site on the surface (see Figure S6). The basis set consisted on double- ζ plus polarization orbitals with an energy-shift of 0.011 Ry for all the atomic species. An energy cut-off of 200 Ry for the real-space grid integrations and $3 \times 3 \times 1$ k -point sampling were considered. The atoms on the topmost Au layer and the molecule were relaxed, until forces were smaller than 0.05 eV/Å.

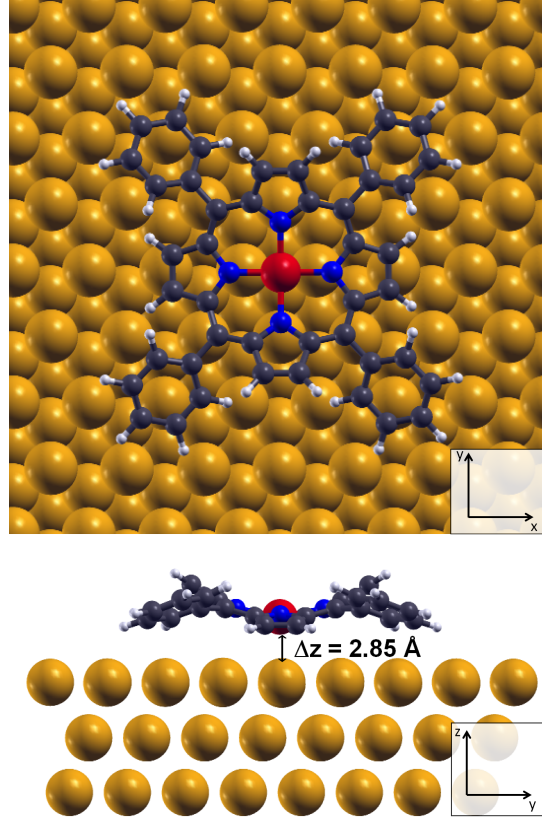


FIG. S6: Top and side view of the optimized geometry of adsorption.

PROJECTED DENSITY OF STATES ON d ORBITALS OF Fe AND PYRROLIC UNITS

Figure S7 shows the projected density of states on the d orbitals of Fe for a wider range than the one shown in Figure 4(a) of the main text. Fully filled curves represent spin up states whereas striped ones represent spin down states. Partial occupations of d_{z^2} , d_{xz} and d_{yz} states can be clearly observed. From this information, it is obtained the scheme of energy levels shown in Figure 4(b) of the main text.

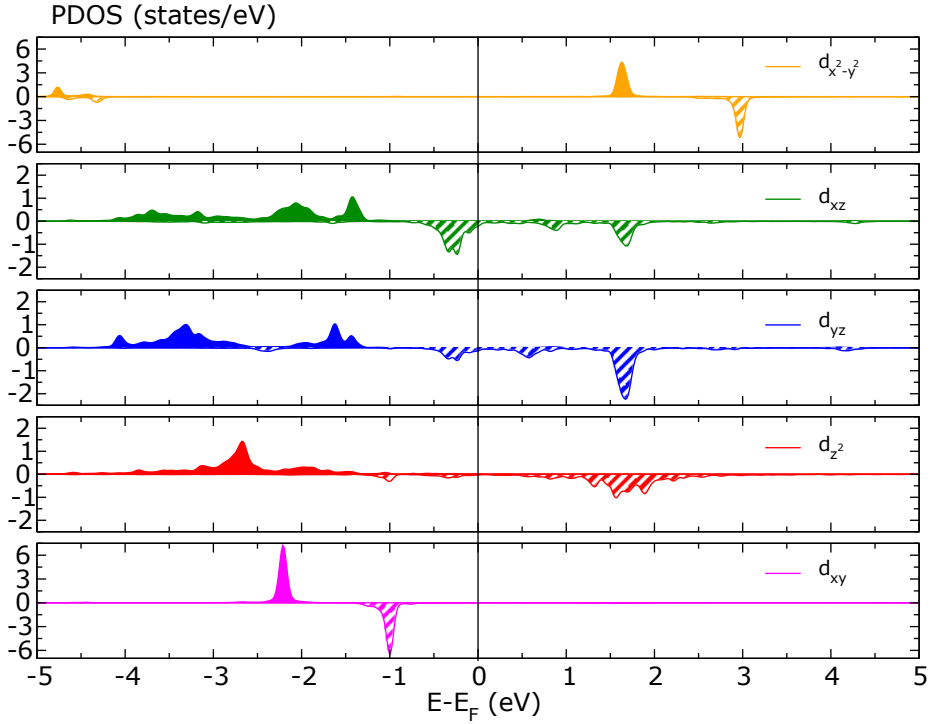


FIG. S7: Projected density of states of the d orbitals of Fe. Positive and negative values represent the majority and minority states.

[S1] D. Gatteschi, R. Sessoli, and J. Villain, *Molecular nanomagnets*, 5 (Oxford University Press, 2006).

[S2] P. W. Anderson, Phys. Rev. **124**, 41 (1961).

[S3] J. R. Schrieffer and P. A. Wolff, Phys. Rev. **149**, 491 (1966).

[S4] M. Ternes, New J. Phys. **17**, 063016 (2015).

[S5] M. Ternes, A. J. Heinrich, and W.-D. Schneider, J Phys Condens Matter **21**, 053001 (2009).

[S6] S. L. Dudarev, G. A. Botton, S. Y. Savrasov, C. J. Humphreys, and A. P. Sutton, Phys. Rev. B **57**, 1505 (1998).

[S7] J. M. Soler, E. Artacho, J. D. Gale, A. García, J. Junquera, P. Ordejón, and D. Sánchez-Portal, J Phys Condens Matter **14**, 2745 (2002).

[S8] J. Klime, D. R. Bowler, and A. Michaelides, J Phys Condens Matter **22**, 022201 (2010).